SOUTHWEST RESEARCH INSTITUTE

August 30,1994

ANNUAL REPORT:

JUPITER THERMOSPHERIC GENERAL CIRCULATION MODEL
NASA GRANT NAGW-3624 SwRI PROJECT #15-5565

Prepared by J. H. Waite, Jr. Southwest Research Institute

This report outlines the progress for the Jupiter Thermospheric General Circulation Model (NASA Grant #NAGW-3624) during the second year of the proposed research. The work during this year has focussed on two central activities: 1) incorporation of subroutine modules into the JTGCM, and 2) determination of modeling inputs from Hubble Space Telescope Faint Object Camera (HST/FOC) and ROSAT images. Both of these activities are discussed briefly below:

1) The initial insertion of Jupiter modules into the existing framework of the TGCM has concentrated so far this year on the inclusion of the major species, their diffusion coefficients, and the inclusion of the complex H_3^+ vibrational chemistry that will serve as the basis for modeling/ data comparisons with the large number of auroral IRTF images. The H_3^+ work was significantly aided by the modeling effort of Yongha Kim et al.(*JGR*,1992) who has served as a consultant on the present work. On the other hand, the major species (H_2, He, H) are taken largely from the one-dimensional modeling work completed in the first year.

A continued area of concentrated effort is the thermal structure and the appropriate lower boundary condition for the hydrocarbon radiative cooling region at the base of the thermosphere (see Clarke et al., *Ap. J. Lett., 430, L73*, 1994). Additional insight was provided by modeling carried out in conjunction with HST/FOC data analysis of an extremely bright aurora with an energy input of over 1 Watt m^{-2}. The one dimensional thermal calculations from the theoretical modeling carried out in conjunction with this work indicate that even moderate heating rates of 0.05 W m^{-2} can result in atmospheric blowoff if the heat is deposited high in the atmosphere (Gerard et al., HST observations of a remarkable UV auroral event on Jupiter, submitted to *Science*, 1994). Such a blowoff could lead to a large hot hydrogen corona over the poles of Jupiter. Furthermore, this work has clarified our ideas on how to approach the lower boundary condition for the thermal structure. We will use a double Bates temperature profile with the lower Bates profile chosen by refitting the synthetic emission spectra for CH_4 and C_2H_2 to the Voyager IRIS data in a manner similar to Drossart et. al, *JGR, 98(E10), 18803*,1993.

2) The aurora at Jupiter is the main energy source responsible for driving thermospheric processes. As such, specification of the morphology of the particle precipitation input, as well as the identity and energy spectrum of the particles, is an extremely important input. Two major works, one nearing completion and one in print, will allow good specification of the required inputs. The first is the analysis of the HST/FOC images acquired by Stern, Waite, McGrath, Trafton, and Gladstone during the Jupiter/Ulysses encounter and by other collaborative HST image data sets with Jean Claude Gerard (whose student Denis Grodent has been visiting us and assisting in this work with this grant providing coverage for his travel). Reconstruction of the auroral morphology from the ROSAT images has necessitated the development of an extensive radiative transfer simulation code that has recently been completed and is presently being used to model and analyze all of the existing HST auroral images. This work will be submitted to the *Journal of Geophysical Research* in October under the title," A new paradigm of Jovian aurora: HST FOC image analysis". This work will allow specification of the first order auroral morphology and energy spectrum of precipitating particles for use in the JTGCM. The second work is the analysis of x-ray auroral images and spectra from Jupiter's auroral zone using ROSAT (Waite et al., *JGR, 99(A8), 14799*, 1994). This work gives important information about the identity and energy spectrum of the auroral particles.

the Sun, Dame et al. (1987) obtained a mean molecular hydrogen density of 0.2 atoms cm^{-3} giving a total hydrogen density of 0.66 atoms cm^{-3}. Our result from the analysis of the isotopic composition of aluminum is therefore consistent with the aluminum isotopes spending most of their lifetime inside the Galactic disk. The recent measurement of the isotopic composition of cosmic-ray Be on the *Voyager 1* and *2* spacecraft gave an average interstellar density of 0.28 atoms cm^{-3} (Lukasiak et al. 1994a). The lower average density deduced from ^{10}Be decay suggests that the Be isotopes may be spending a larger fraction of their time in regions of density less than 0.66 atoms cm^{-3}. Since the two isotopes ^{26}Al and ^{10}Be have essentially the same origin in the matter disk of the Galaxy (with an average density ~ 0.66 atoms cm^{-3}), any difference in the deduced interstellar density suggests to us that the longer lived ^{10}Be secondaries are diffusing farther away from the disk and thus encountering a lower average density. If this 1 σ difference in the average interstellar density is confirmed by more precise measurements in the future, it would favor a halo model for the confinement region of cosmic rays where the propagation region extends beyond the matter disk of the Galaxy, rather than an explanation of the different densities (or different surviving fractions) derived from ^{26}Al and ^{10}Be as being due, for example, to a clumpy interstellar medium. This argument can in fact be made quantitative by considering the disk halo diffusion model discussed by Webber, Lee, & Gupta, 1992. For the case where the convection velocity away from the disk = 0 we show in Figure 4 the expected surviving fractions for both ^{10}Be and ^{26}Al as a function of the halo size. Using the *Voyager* data only, for ^{26}Al the deduced halo thickness is 1.9 (+1.4, −1.0) kpc, as compared with 2.8 (+1.2, −0.9) kpc deduced earlier from ^{10}Be measurements (Lukasiak et al. 1994a). Using the average of all available spacecraft data on ^{26}Al and ^{10}Be gives $f = 0.28 \pm 0.07$ and 0.21 ± 0.04, respectively. These values lead to roughly the same halo thickness of 2.3 (+1.0, −0.6) kpc for both ^{26}Al and ^{10}Be. These latter data points are shown as open circles in Figure 4. The consistency of the halo size as derived from the ^{26}Al and ^{10}Be measurements is a measure of our understanding of the diffusion of cosmic rays perpendicular to the Galactic disk into the halo.

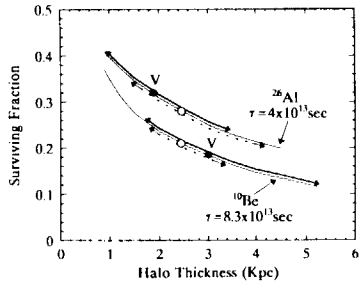

FIG. 4.—Surviving fraction of ^{26}Al at ~ 400 MeV nucleon^{-1} calculated as a function of halo size (*thin solid line*) by Webber, Lee, & Gupta (1992). The solid points correspond to *Voyager* measurements and the open circles correspond to the average of all available spacecraft data on ^{26}Al and ^{10}Be, respectively. The arrows at the end points of a thick solid line mark the region corresponding to the error in surviving fraction obtained in *Voyager* measurements. The dotted lines mark the region corresponding to the average values.

This work was supported in part by JPL contract FCPO 988724.

REFERENCES

Dame, T. M., et al. 1987, ApJ, 322, 706
Ferrando, P., et al. 1988, Phys. Rev. C, 37, 1490
———. 1991, A&A, 247, 163
Garcia-Munoz, M., Simpson, J. A., & Wefel, J. P. 1981, Proc. 17th ICRC (Paris), 2, 72
Gleeson, L. F., & Axford, W. I. 1968, ApJ, 154, 1011
Lukasiak, A., Ferrando, P., McDonald, F. B., & Webber, W. R. 1994a, ApJ, 423, 426
———. 1994b, ApJ, 426, 366
Shull, J. M., & Van Steenberg, M. E. 1985, ApJ, 294, 599
Simpson, J. A., & Garcia-Munoz, M. 1988, Space Sci. Rev., 46, 205
Stone, E. C., et al. 1977, Space Sci. Rev., 46, 205
Webber, W. R. 1982, ApJ, 252, 386
Webber, W. R., Kish, J., & Schrier, D. 1990a, Phys. Rev. C, 41, 520
———. 1990b, Phys. Rev. C, 41, 533
———. 1990c, Phys. Rev. C, 41, 547
Webber, W. R., Kish, J. C., & Schrier, D. A. 1985, Proc. 19th ICRC Conf. Papers, 2, 88
Webber, W. R., Lee, M. A., & Gupta, M. 1992, ApJ, 390, 96
Wiedenbeck, M. E. 1983, Proc. 18th ICRC Conf. Papers, 9, 147
Wiedenbeck, M. E., & Greiner, D. E. 1980, ApJ, 239, L139
Young, J. S., Freier, P. S., & Waddington, C. J. 1979, Proc. 16th ICRC Conference Papers, 1, 442

THE ASTROPHYSICAL JOURNAL, 430:L73–L76, 1994 July 20

HUBBLE SPACE TELESCOPE GODDARD HIGH-RESOLUTION SPECTROGRAPH H_2 ROTATIONAL SPECTRA OF JUPITER'S AURORA

JOHN T. CLARKE,[1] LOTFI BEN JAFFEL,[2] ALFRED VIDAL-MADJAR,[2] G. RANDALL GLADSTONE,[3] J. HUNTER WAITE, JR.,[3] RENEE PRANGÉ,[4] JEAN-CLAUDE GÉRARD,[5] JOE AJELLO,[6] AND GEOFFREY JAMES[6]

Received 1994 March 16; accepted 1994 May 4

ABSTRACT

We have observed the emission spectrum from Jupiter's north auroral atmosphere with 0.57 Å spectral resolution over 1204–1241 Å. Bright emissions have been detected from 50° to 60° latitude at locations consistent with 6 to 30 R_J auroral ovals, with much fainter emissions away from the auroral ovals. The emission spectrum is well fitted by both laboratory spectra and theoretical models of optically thin electron excited H_2, with added Doppler-broadened Lyα emission. The observed Lyα emission wings extend more than 1 Å from line center and appear correlated in strength with the H_2 brightness. Individual rotational lines in the H_2 Werner band system are resolved, allowing a determination of the H_2 rotational temperature at the altitude of the emission. We derive best-fit temperatures from 400–450 to 700–750 K, with the auroral emission layer temperature changing either across the auroral oval or over several days' time. These observations demonstrate for the first time the ability to measure the observed rapid H_2 temperature variations across Jupiter's auroral atmosphere.

Subject headings: planets and satellites: general — planets and satellites: individual (Jupiter)

1. INTRODUCTION

A polar aurora energetically dominates Jupiter's upper atmosphere with a deposited power of 10^{13}–10^{14} W: the larger value is 20–50 times greater than the global solar UV flux absorbed at the same altitudes. This is 100–1000 times the average Earth aurora energy and is believed to produce extreme conditions in Jupiter's auroral ionosphere and thermosphere as well as dominating the global thermospheric circulation. Spectra of Jupiter's auroral H Lyα and H_2 Lyman and Werner bands were first obtained in 1979 spring with the *Voyager* UVS (Broadfoot et al. 1979) and *IUE* (Clarke et al. 1980). Short-term UVS and long term *IUE* studies show consistent emission maxima near System III longitudes 180°–200° in the north and 0°–50° in the south (Skinner et al. 1984; Herbert, Sandel, & Broadfoot 1987; Livengood, Strobel, & Moos 1990; Harris, Clarke, & McGrath 1994), in contrast with the solar wind driven pattern of the Earth's aurora, which is fixed in local time. *Hubble Space Telescope* (*HST*) Faint Object Camera (FOC) UV images have shown bright narrow arcs of emission at high latitudes (Gérard et al. 1993, 1994) corresponding to field lines crossing the equatorial plane at 30 Jovian radii (R_J) in the O6 magnetic field model (Connerney 1992). IR auroral observations give hydrocarbon temperatures 180–500 K over 1–0.001 mbar, and H_3^+ values of 900–1500 K over 0.1 and 0.001 μbar, implying a rapid increase in temperature with altitude (Drossart et al. 1993). The UV auroral emission is believed to be at intermediate altitudes near the hydrocarbon homopause from modeled hydrocarbon absorption of the UV auroral emission (Yung, et al. 1982; Gladstone & Skinner 1989; Livengood et al. 1990). Despite rapid progress in recent years, many fundamental questions about Jupiter's aurora remain unanswered, including the detailed morphology, time variability, the identity, source, and number of precipitating particles, the particle acceleration mechanisms, the amount of Joule heating, and the effects on atmospheric dynamics and chemical composition. We have obtained high-resolution spectra to determine more accurately the physical conditions in Jupiter's auroral atmosphere.

2. OBSERVATIONS

Spectra of Jupiter were obtained over 1993 May 28 to June 3 with the Goddard High-Resolution Spectrograph (GHRS) on *HST*, with grating G160M and the 2 arcsec square aperture. The aperture was held fixed on Jupiter's central meridian at a constant latitude, and the central meridian longitudes (CML) observed in the aperture (Fig. 1) from the extent of the aperture and planetary rotation are listed in Table 1. Pointing was by direct offset from guide stars, with an estimated uncertainty of 1″ based on statistics of GHRS acquisitions of stellar sources. The wavelength range 1204–1241 Å covers the H Lyα emission and H_2 Werner ($C\,^1\Sigma_u^- - X\,^1\Sigma_g^+$) band emissions. H_2 Lyman band emissions are also present but are relatively weak in this wavelength range. Due to the brightness of the observed emissions, standard Space Telescope Science Institute (STScI) reduction procedures are sufficient and have been used for all spectra reported here. A full analysis of the H Lyα emission will require a detailed model and subtraction of the geocoronal emission, which is not resolved from Jupiter's emission, and this work will be reported at a later date.

The six observed spectra are plotted in Figure 2. Since point sources are resolved within the aperture, the observed width of the H_2 emission bands contains information about both the intrinsic spectral width of the bands and the spatial extent of

[1] AOSS Department, University of Michigan, Ann Arbor, MI 48109-2143.
[2] Institut d'Astrophysique de Paris, 98 bis Boulevard Arago, 75014 Paris, France.
[3] Southwest Research Institute, 6220 Culebra Road, San Antonio, TX 78238.
[4] Institute d'Astrophysique Spatiale, Université Paris XI, 91405 Orsay Cedex, France.
[5] Institut d'Astrophysique, Université de Liège, Avenue de Cointe, 5, B-4000 Liège, Belgium.
[6] MS 183/601, Jet Propulsion, 4800 Oak Drive, Pasadena, CA 91109.

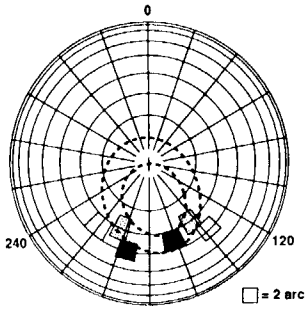

FIG. 1.—Projected aperture locations on polar projection of Jupiter at times of Goddard High-Resolution Spectrograph (GHRS) G160M spectra. Aperture is 2 arcsec square, and appears elongated due to planet rotation and the geometry of projection. Model auroral ovals are for 6 and 30 R_J in the O6 magnetic field model (Connerney 1992). Darker shading qualitatively indicates the H_2 brightness.

the emitting region in the aperture. We have determined the point-spread function (PSF) for diffuse emission filling the aperture from spectra looking down at sunlit geocoronal H Lyα emission, which gives a rectangular shape with a full width at half-maximum of 0.57 Å compared with the point source resolution of 0.11 Å. A co-addition of the brightest Werner band features gives a profile which is consistent in width and shape with this PSF, implying that the H_2 emission region also fills the aperture and that the intrinsic width of the emission bands is small compared with 0.57 Å. The detection of comparably bright emissions over a range of 10° latitude and 70° longitude implies a partially diffuse emission region, although we cannot derive the exact spatial distribution from these limited data and there may also be discrete bright features. The observed spatial distribution of H_2 brightness (Fig. 1) is consistent with auroral emission over an extended region, requiring some emission down to the 6 R_J oval and also up to the 30 R_J oval and suggesting little emission equatorward of the 6 R_J oval. With a 1 arcsec pointing uncertainty, however, an accurate mapping of the auroral emission region is not possible, and we also have a time-averaged picture over a period of 7 days.

Comparing the brightest spectrum in each of the three pairs, the total H_2 emission brightnesses are similar, although there are differences in the relative strengths of features. Both +60 spectra have a more uniform relative brightness of the individual lines than the +50 and +55 spectra. There is also little broadening at the base of the Lyα line in spectra with weak H_2 emission (e.g., Jup + 50 130°–141°), while there is pronounced wing emission in spectra with bright H_2 emission, as first observed with *IUE* (Clarke, Trauger, & Waite 1989). The Lyα wing emission intensity appears correlated with H_2 intensity and is also greater in both +60 spectra (e.g., Jup + 60 140°–151°), although the present data set is not sufficient to establish statistical correlations. We have looked for short-term changes by dividing each of the H_2 spectra into four equal time segments: within the higher noise level in the shorter spectra we have not found significant variations. H_2 emission brightnesses over 1204–1241 Å are listed in Table 1, assuming the aperture is filled (2" emission region). Assuming the average color ratio of 2.46 (Livengood et al. 1990; Harris et al. 1994) corresponding to 50% absorption by CH_4, we multiply by 17 to extrapolate to the integrated H_2 emission over 1150–1650 Å for comparison with *IUE* brightnesses (in an assumed 2" by 9" region).

TABLE 1

HST GHRS G160M SPECTRA OF JUPITER'S NORTH AURORA*

Date (1993)	Time (UT)	Latitude	Longitude (CML)	H_2 4πI (kR) (1204–1241 Å)	H_2 4πI (kR) (1150–1650 Å)
May 28	11:55	+50	130–141	≤1.5	≤25
May 28	13:31	+50	188–199	7.1	120
June 1	15:26	+60	140–151	10.3	174
June 1	17:04	+60	199–210	2.9	49
June 3	7:36	+55	159–170	10.1	171
June 3	9:13	+55	215–226	5.8	98

* All spectra were 1088 s long; listed times indicate start of exposure.

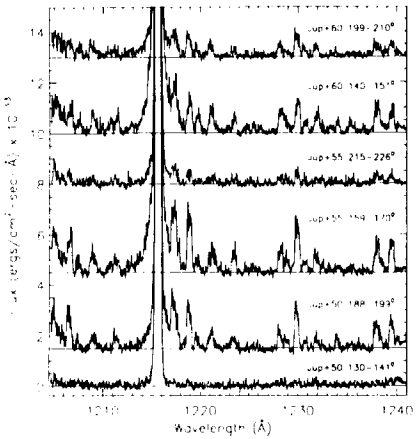

FIG. 2.—Sequence of GHRS G160M spectra at locations indicated in Table 1 and Fig. 1, with vertical offsets for clarity. In each spectrum label "Jup + x y z," x = latitude and y–z = longitude range (System III) of the aperture on the central meridian. Note the correlation between H_2 band intensity and Lyα wing intensity.

3. DISCUSSION

Figure 3 compares the bright Jupiter + 50 spectrum with laboratory and synthetic spectra at two temperatures. Laboratory UV spectra have been obtained in an electron impact collision chamber operating in the crossed-beam mode, in which a magnetically collimated beam of electrons is crossed with a gas beam from a capillary array (Ajello, James, & Franklin 1989). The background gas pressure was 2×10^{-5} torr and the electron beam current was 100 μA. Emission cross sections for the Lyman and Werner bands at 100 eV electron energy are from Ajello et al. (1988). When the Jupiter spectra are degraded to the 0.9 Å resolution of the laboratory spectra, the agreement is excellent with each feature appearing in the laboratory spectrum. The 100 eV energy in the laboratory and models represents the energy of exciting secondary electrons, and this comparison does not provide information on the composition of the primary particles in Jupiter's aurora.

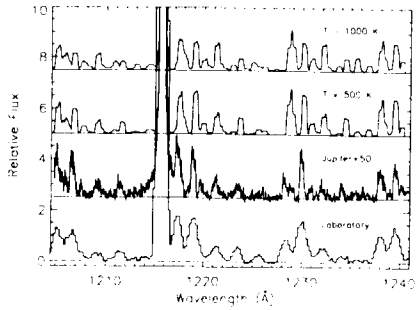

FIG. 3.—Comparison of +50° latitude auroral spectrum with laboratory and model spectra. The laboratory spectrum is for 100 eV electrons on H_2 gas with 0.9 Å resolution, while the model spectra for T = 500 and 1000 K have been convolved with the 0.57 Å G160M point-spread function.

Synthetic spectra have been calculated for electron impact of ground state H_2 ($X\,^1\Sigma_g^+$), assuming a Boltzmann distribution in the rotational and vibrational levels of the X state, and convolved with the G160M PSF. The intensity in each rotational line of the Lyman and Werner bands is obtained from the assumption of steady state between the population and the emission rates of the rotational levels of the B and C states. Direct excitation from the X to the B and C states is assumed proportional to the optical band strength, with appropriate Honl-London factors. Cascading from the (E, F) to the B state is included, adopting the cross sections to the B, C, and (E, F) states measured by Ajello et al. (1984) for 100 eV electron excitation. The intensity distribution among the lines within the Lyman and Werner bands reflects the rotational temperature (assumed equal to the kinetic temperature) of the gas in the emitting region. The synthetic spectra show features at all wavelengths of observed features, and from this comparison we have identified the brightest transitions (Table 2). There are some differences between the relative feature intensities, the most obvious at 1228.3 Å, where the model intensity appears too large. Since the laboratory spectrum fits the observed line ratios rather well, we assume this represents a shortcoming in the model. The nature of this difference is under investigation.

To determine the best-fit temperature, we perform a least-squares fit of the synthetic spectra with the brighter observed spectrum from each day. Synthetic spectra are generated for 200 to 1200 K and the χ^2 residual $1/N[\Sigma(I_i^s - I_i^o)]^{1/2}$ is calculated and minimized, where N is the number of spectral points and I_i^s and I_i^o are the intensities in the synthetic and observed spectra, respectively. Since none of the observed transitions connect to the ground state and the fraction of vibrationally excited H_2 above the emitting region is estimated to be less than 1% (Cravens 1987), the emission is assumed to be optically thin. The synthetic spectra include the Werner and Lyman band systems excluding regions ±1.5 Å of the Lyα line and ±0.8 Å of the 1228.3 Å feature. We have also run spectra with just Werner bands and including the 1228.3 Å feature,

TABLE 2

SPECTRAL IDENTIFICATIONS OF BRIGHT H_2 FEATURES

Wavelength (Å)	Spectroscopic Identification*	Identification Wavelength (Å)	Relative Strength (at 500 K)
1205.0	C–X (1,5) R1	1205.1	4.46
	C–X (1,5) R0	1205.5	1.65
1206.3	C–X (1,5) Q1	1206.8	6.67
	C–X (1,5) Q2	1207.7	1.84
1209.0	C–X (1,5) Q3	1209.1	2.72
1211.2	C–X (1,5) P3	1211.6	2.98
1217.2	C–X (2,6) R1	1217.5	7.27
	C–X (2,6) R0	1217.9	2.68
1219.0	C–X (2,6) Q1	1219.1	10.9
	C–X (2,6) Q2	1220.0	3.00
1221.1	C–X (2,6) Q3	1221.3	4.42
1223.5	C–X (2,6) P3	1223.7	4.85
1228.3	C–X (3,7) R1	1228.6	7.44
	C–X (3,7) R0	1229.0	2.74
1230.1	C–X (3,7) Q1	1230.2	11.1
	C–X (3,7) Q2	1231.0	3.07
1232.0	C–X (3,7) Q3	1232.1	4.52
1234.0	C–X (3,7) P3	1234.5	4.96
1238.0	C–X (4,8) R1	1238.0	5.93
	C–X (4,8) R0	1238.4	2.19
1239.7	C–X (4,8) Q1	1239.5	8.86
	C–X (4,8) Q2	1240.2	2.45
	C–X (4,8) Q3	1241.3	3.61

* C–X (Werner system), (v', v''), rotational branch.

with very similar results in temperature, although slightly poorer fits. The χ^2 values are plotted in Figure 4, from which we derive best-fit temperatures of 400–450 K for the +50 and +55 latitude spectra and 700–750 K for the +60 latitude spectrum. Note that although the overall fit is clearly better for the +60 spectrum, the +60 fit is less well defined in temperature than the others (i.e., a lower χ^2 but broader curve with temperature). The poor definition in temperature in all three spectra may in part reflect the presence of more than one temperature component in the 2" aperture, including possible variations in the H_2 temperature with either position or altitude.

The above results imply a doubling in H_2 auroral temperature either over several days' time or with location. A variation with latitude might represent either a bulk heating or

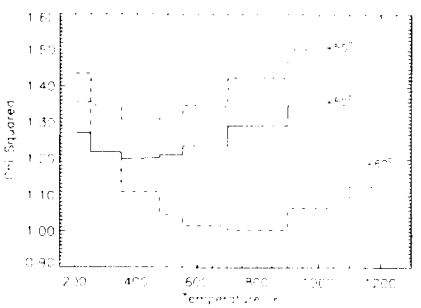

FIG. 4.—Values of χ^2 for model fits to the brightest spectra at each latitude; see text for description of method.

an increase in altitude of the auroral layer, since the temperature increases rapidly with altitude: this, in turn, would imply a higher altitude aurora from softer precipitating particles. Similar arguments may be applied to changes with time of the auroral primary particle energy. In the modeled temperature/altitude profile of Drossart et al. (1993), temperatures of 400–750 K occur just above the homopause, where temperature is increasing rapidly with altitude. This places the peak UV auroral emission within or above the IR hydrocarbon emissions at 5–10 μm and below the ionospheric H_3^+ emissions at 2–4 μm, consistent with the altitude derived from models of CH_4 absorption of the UV emission. Note that over the 40 Å range observed here, the CH_4 absorption cross section is nearly constant with wavelength. The four brightest GHRS spectra (Table 1) are within the range of auroral brightnesses observed with *IUE* (Livengood et al. 1990; Harris et al. 1994). GHRS spectra of Jupiter have also been reported by Trafton et al. (1994) with similar modeling of H_2 emission spectra but over different wavelength ranges. They observed at 180° CML and +67° latitude, placing the aperture just poleward of the 30 R_J oval, and report brightnesses roughly 10 times less than those reported here. Although variability between the observations cannot be ruled out, the complete set of observations suggest that the auroras are much fainter poleward of the 30 R_J oval.

4. CONCLUSIONS

We report *HST*/GHRS spectra of Jupiter's north auroral zone revealing bright H_2 emissions concentrated between the 6 to 30 R_J auroral ovals. The emission spectrum is well fitted by laboratory spectra of 100 eV electron excitation of H_2, consistent with excitation by secondary electrons independent of the composition of the primary particles. Synthetic spectra of H_2 emission give best fits from 400–450 to 700–750 K, indicating a temperature change of the auroral emission layer either over a few days time or with location. The auroral H Lyα emission has strong Doppler wings not present in the laboratory spectra: the wing emission intensity appears correlated with the H_2 emission intensity and relatively stronger in the spectra which have the highest temperatures. Although these spectra demonstrate the determination of the auroral H_2 temperature with moderate spectral and spatial resolution, better temporal coverage will be required to identify quantitative relationships between emission intensities, temperatures, emission altitudes, etc.

We acknowledge assistance from the STScI in scheduling and reducing the *HST* observations, and J. T. C. thanks the Instituts d'Astrophysique de Paris and d'Astrophysique Spatiale in Orsay for hospitality during 1993 fall. The research was supported by grants GO-3511.01-91A from STScI and NAGW-1766 from NASA to the University of Michigan. J. C. G. is supported by the Belgian Foundation for Scientific Research and acknowledges funding by the PRODEX ESA program of the Belgian Science Policy Office. This work is based on observations with the NASA/ESA *HST*, obtained at the STScI, which is operated by the AURA, Inc., for NASA under contract NAS 5-26555.

REFERENCES

Ajello, J. M., James, G. K., & Franklin, B. O. 1989, Phys. Rev., 40, 890
Ajello, J. M., Shemansky, D., Kwok, T. L., & Yung, Y. L. 1984, Phys. Rev. A, 29, 636
Ajello, J. M., et al. 1988, Appl. Opt., 27, 890
Broadfoot, A. L., et al. 1979, Science, 204, 979
Clarke, J. T., Moos, H. W., Atreya, S. K., & Lane, A. L. 1980, ApJ, 241, L179
Clarke, J. T., Trauger, J., & Waite, J. H., Jr. 1989, Geophys. Res. Lett., 16, 587
Connerney, J. E. P. 1992, in Planetary Radio Emission, Vol. 3, ed. H. Rucker, M. L. Kaiser, & S. J. Bauer (Vienna: Austrian Academy of Science Press), 13
Cravens, T. E. 1987, J. Geophys. Res., 92, 11083
Drossart, P., Bezard, B., Atreya, S., Bishop, J., Waite, J. H., Jr., & Boice, D. 1993, J. Geophys. Res., 98, 18803
Gérard, J.-C., Dols, V., Paresce, F., & Prangé, R. 1993, J. Geophys. Res., 98, 18793
Gérard, J.-C., et al. 1994, Planet. Space Sci., submitted
Gladstone, G. R., & Skinner, T. E. 1989, in Proc. Flagstaff Workshop on Time Variable Phenomena in the Jovian System, ed. M. J. S. Belton, R. A. West, & J. Rahe (NASA SP-494), 221
Harris, W. M., Clarke, J. T., & McGrath, M. A. 1994, Icarus, submitted
Herbert, F., Sandel, B. R., & Broadfoot, A. L. 1987, J. Geophys. Res., 92, 3141
Livengood, T. A., Strobel, D. F., & Moos, H. W. 1990, J. Geophys. Res., 95, 10375
Skinner, T. E., et al. 1984, ApJ, 278, 441
Trafton, L., Gérard, J.-C., & Waite, J. H., Jr. 1994, ApJ, 421, 816
Yung, Y. L., Gladstone, G. R., Chang, K. M., Ajello, J. M., & Srivistava, S. K. 1982, ApJ, 254, L65

THE ASTROPHYSICAL JOURNAL, 430:L77–L80, 1994 July 20

PREDICTIONS OF OXYGEN ISOTOPE RATIOS IN STARS AND OF OXYGEN-RICH INTERSTELLAR GRAINS IN METEORITES

ARNOLD I. BOOTHROYD
Canadian Institute for Theoretical Astrophysics, University of Toronto, 60 St. George Street, Toronto, Ontario, Canada M5S 1A7
I.-JULIANA SACKMANN
W. K. Kellogg Radiation Laboratory 106-38, California Institute of Technology, Pasadena, CA 91125
AND
G. J. WASSERBURG
Lunatic Asylum, Charles Arms Laboratory 170-25, Division of Geological and Planetary Sciences, California Institute of Technology, Pasadena, CA 91125
Received 1994 March 16, accepted 1994 April 29

ABSTRACT

We carried out detailed, self-consistent calculations for stars from 1 to 9 $M_\odot$ over a wide range of metallicities, following the evolution and nucleosynthesis from the pre main sequence to the asymptotic giant branch (AGB), in order to provide a self-consistent grid for evaluating stellar oxygen isotopic variations. These were calculated for first and second dredge-up, and for some masses also for third dredge-up and "hot bottom" convective envelope burning on the AGB. We demonstrate that $^{16}O/^{17}O$ in red giant envelopes is primarily a function of the star's mass, while $^{16}O/^{18}O$ is primarily a function of the initial composition. Uncertainties in the ^{17}O-destruction rate have *no effect* on the $^{16}O/^{17}O$ ratio for stars from 1 to 2.5 $M_\odot$, but *do affect* the ratios for higher masses: the stellar $^{16}O/^{17}O$ observations are consistent with the Landré et al. (1990) rates using $f = 0.2$ for $^{17}O(p, \gamma)^{18}F$ and $^{17}O(p, \alpha)^{14}N$, and with the Caughlan & Fowler (1988) rates using $f \approx 1$. The stellar $^{16}O/^{18}O$ observations require $f \approx 0$ in the Caughlan & Fowler $^{18}O(p, \alpha)^{15}N$ rate.

First dredge-up has the largest effect on the oxygen isotope ratios, decreasing $^{16}O/^{17}O$ significantly from the initial value and increasing $^{16}O/^{18}O$ slightly. *Second* and *third dredge-up* have only minor effects for solar metallicity stars. The absence of very low observed $^{16}O/^{18}O$ ratios is consistent with a major increase in the $^{18}O(\alpha, \gamma)^{22}Ne$ rate over the Caughlan & Fowler (1988) value. *Hot bottom burning* in stars above about 5 $M_\odot$ can cause a huge increase in $^{16}O/^{18}O$ (to $\gtrsim 10^6$), and possibly a significant decrease in $^{16}O/^{17}O$; these are accompanied by a huge increase in ^7Li and a value of $^{12}C/^{13}C \approx 3$.

The oxygen isotope ratios in the Al_2O_3 grains (Orgueil grain B, the Murchison 83-5 grain, and the new Bishunpur B39 grain) can be accounted for *if they originated in stars that did NOT have the same initial* $^{16}O/^{18}O$ *ratio*. Thus one *cannot* assume uniform isotope ratios, even for stars of nearly solar composition. The grains' $^{16}O/^{17}O$ ratios, together with the ^{26}Mg excesses that indicate grain formation in a ^{26}Al-rich environment, indicate that the Orgueil grain B and Murchison 83-5 grain originated in stars of roughly 1.5 $M_\odot$, during third dredge-up on the AGB. The new Bishunpur B39 grain originated in a star of either 2 or of 4–7 $M_\odot$.

Subject headings: dust, extinction — nuclear reactions, nucleosynthesis, abundances — stars: abundances — stars: AGB and post-AGB — stars: giants

1. INTRODUCTION

It is only in the last few years that intact interstellar grains that originated from stars have been isolated from meteorites. These meteoritic grains permit direct laboratory study of their physical and chemical nature. The first such grains found were carbon-rich (Lewis et al. 1987; Bernatowicz et al. 1987; Amari, Lewis, & Anders 1990). Oxygen-rich interstellar grains are more difficult to isolate. Nonetheless, three such oxygen-rich (Al_2O_3) grains have recently been discovered, having oxygen isotope ratios totally different from solar system values. The first such grain was Orgueil grain B (Huss et al. 1992, 1993; Hutcheon et al. 1994); it was enriched by more than a factor of 2 in ^{17}O but had an approximately solar $^{16}O/^{18}O$ ratio. The second grain, Murchison 83-5 (Nittler et al. 1993), had a similar ^{17}O enrichment and was also somewhat depleted in ^{18}O. A third grain, Bishunpur B39, has just been discovered (see companion *Letter*: Huss et al. 1994); it has even more extreme ^{17}O enrichment (a factor of ~ 7) and the largest ^{18}O depletion of the three grains (nearly a factor of 2). This *Letter* presents the results of detailed self-consistent calculations of stellar evolutionary models and their nucleosynthesis, providing the oxygen isotope ratios of stellar surface layers at crucial points in the stars' lifetimes as a function of stellar mass, in order to ascertain the astrophysical site where these grains originated.

2. METHODS

We considered stars of masses from 0.85 to 9 $M_\odot$, with metallicities $Z = 0.025$, 0.02, 0.016, 0.01, 0.0044, 0.001, and 0.0001 (see also Boothroyd & Sackmann 1994); for evolutionary program details, see Boothroyd & Sackmann (1988) and Sackmann, Boothroyd, & Fowler (1990). For all runs, we used a helium mass fraction $Y = 2Z + 0.24$. For $Z = 0.02$, we used $C/Z = 0.2179$, $N/Z = 0.0531$, and $O/Z = 0.4816$ (by mass) as in Keady (1985), and similar to Ross & Aller (1976) and Grevesse (1984); we used solar system values of $^{16}O/^{17}O = 2660$ and $^{16}O/^{18}O = 500$ (by number). For some runs, we

DOC #: 22349 ABSTRACT SCREEN PAGE: 1 ** WORDS NOT FOUND *

Jupiter thermospheric general circulation model

ABQ: NC
ABA: Author

CIN: BGB
KIN: TLM
AIN:

This report outlines the progress for the Jupiter Thermospheric General Circulation Model (NASA Grant NAGW-3624) during the second year of the proposed research. The work during this year has focused on two central activities: (1) incorporation of subroutine modules into the JTGCM, and (2) determination of modeling inputs from Hubble Space Telescope Faint Object Camera (HST/FOC) and ROSAT images. Both of these activities are discussed briefly.

JTGCM

PF1=ABA LIST; PF2=RESET; PF3=SIGNON; PF4=RELEASE FROM SUBQ; PF5=SELECTION;
PF6=SUBQUEUE; PF7=STORE ABSTRACT; PF8=MAI; PF10=SEND TO 'MAIQ';
PF14=PREVIOUS PAGE; PF15=NEXT PAGE; PF19=TITLE-EXT; PF20=INDEX TERMS
4B• A =-•PC LINE 11 COL 2

DOC NUMBER: 22349 INDEXING: SUBJECT/TERMS SCREEN CIN: BGB
TITLE: Jupiter thermospheric general circulation model KIN: TLM
AIN:

	MAJOR TERMS:	SWITCH
1:	THERMOSPHERE	_
2:	ATMOSPHERIC GENERAL CIRCULATION MODELS	_
3:	ROSAT MISSION	_
4:	JUPITER (PLANET)	_
5:	MATHEMATICAL MODELS	_
6:	THERMAL ANALYSIS	_
7:		_
8:		_
9:		_
10:		_
11:		_
12:		_
13:		_
14:		_
15:		_

	MINOR TERMS:	
1:	HUBBLE SPACE TELESCOPE	_
2:	FAINT OBJECT CAMERA	_
3:	ROTATIONAL SPECTRA	_
4:	IMAGE ANALYSIS	_
5:		_
6:		_
7:		_
8:		_
9:		_
10:		_
11:		_
12:		_
13:		_
14:		_
15:		_

PROPOSED TERMS:

PF2=RESET; PF3=SIGNON; PF4=RELEASE; PF5=SELECTION; PF6=SUBQ
PF10=ALPHA; PF11=HIERARCHY; PF12=STORE; PF13=CENTRAL SCREEN; PF20=TITLE/WNF
4B• A =-•PC LINE 6 COL 11